Available online at www.sciencedirect.com
ScienceDirect
Communications in Nonlinear Science and Numerical Simulation 14 (2009) 160–173
Communications in Nonlinear Science and Numerical Simulation
www.elsevier.com/locate/cnsns

# Hydrocarbon microtremors interpreted as nonlinear oscillations driven by oceanic background waves

R. Holzner [a,*], P. Eschle [a], S. Dangel [a,d], M. Frehner [b], C. Narayanan [c], D. Lakehal [c]

[a] Spectraseis Technologie AG, Zurich, Switzerland
[b] Department of Earth Sciences, ETH, Zurich, Switzerland
[c] ASCOMP GmbH, Zurich, Switzerland
[d] Remote Sensing Laboratories, University of Zurich, Switzerland

Received 19 December 2006; received in revised form 30 May 2007; accepted 27 June 2007
Available online 24 August 2007

**Abstract**

Characteristic low frequency seismic signals have been observed in areas where hydrocarbon reservoirs are present. A possible interpretation is the excitation of hydrocarbon related resonances. Basic models of an oscillating liquid filled porous medium are investigated. Synthetic spectra of the ab initio Navier–Stokes equations and of basic linear and nonlinear one-dimensional oscillators show characteristic features of measured spectra when oceanic background waves around 0.1–0.2 Hz are assumed to be the external driving force.


*PACS:* 47.10.ad; 05.45.−a; 93.85.Tf; 91.55.Ax

*Keywords:* Navier–Stokes equations; Nonlinear dynamics; Oil prospecting; Mechanics, theory and modelling in geophysics

## 1. Introduction

Hydrocarbon microtremor analysis (HyMAS) [1,2] is an innovative seismic spectroscopy technology identifying the hydrocarbon content of geological structures by analyzing low frequency background wave signals. Hydrocarbon indicating information is extracted from spectral modifications of naturally occurring background waves in the 0.1–20 Hz range interacting with hydrocarbon bearing porous structures. Similar observations have been made at more than 15 sites worldwide [3–8].

The first consistent report on low frequency seismic measurements and analysis to investigate the hydrocarbon content of geological formations was given in 2001 by Dangel et al. [3]. A linear relationship between the observed signal and the total thickness of hydrocarbon layers was established by various measurements that

* Corresponding author. Tel.: +41 44 312 15 63.
*E-mail address:* reto.holzner@hispeed.ch (R. Holzner).

1007-5704/$ - see front matter © 2007 Published by Elsevier B.V.
doi:10.1016/j.cnsns.2007.06.013

were compared to well log data mainly in the Middle East. Earlier on in 1993 other findings of low frequency seismic signals were related to oil-saturated layers by Goloshubin et al. [4]. They analyzed experimental cross-hole seismic data from a field in West Siberia and found very low frequency (10 Hz), very low velocity (300 m/s) and high amplitude "slow wave" signals inside oil-saturated layers.

Similar potentially hydrocarben related low frequency seismic spectrum modifications have been observed by several groups recently. Al Dulaijan et al. [5] have reported the occurrence of such signals during a the comparison of different novel exploration techniques applied in the Rub Al-Khali Desert of Saudi Arabia while Rached, Suntsov et al., Akrawi and Kouznetsov et al. [6,7] found similar occurrences in Kuwait, Russia and the Arabian Peninsula.

From recent land surveys in Brazil [8] typical HyMAS data of a weak and a strong signal indicating low and high hydrocarbon potential are shown in Fig. 1.

A general approach towards an explanation of such behaviour is the phenomenological interpretation as a driven linear or nonlinear oscillator [9].

The straight forward approach to describe such observations is the general equation for a one-dimensional nonlinear oscillator

$$\frac{d^2x}{dt^2} + \frac{b}{m}\frac{dx}{dt} + \omega_0^2 x(1 + Ax + Bx^2) = \frac{F}{m}\sin(\Omega t) \tag{1}$$

with space variable $x$, frictional damping term $b/m$, resonance frequency $\omega_0$, driving acceleration amplitude $F/m$ and driving frequency $\Omega$, which already leads to a remarkably good fit as displayed in Fig. 1. The input excitation $F/m$ at the ocean wave peak frequency of $\Omega = 2\pi \cdot 0.22$ Hz generates a second harmonic at about

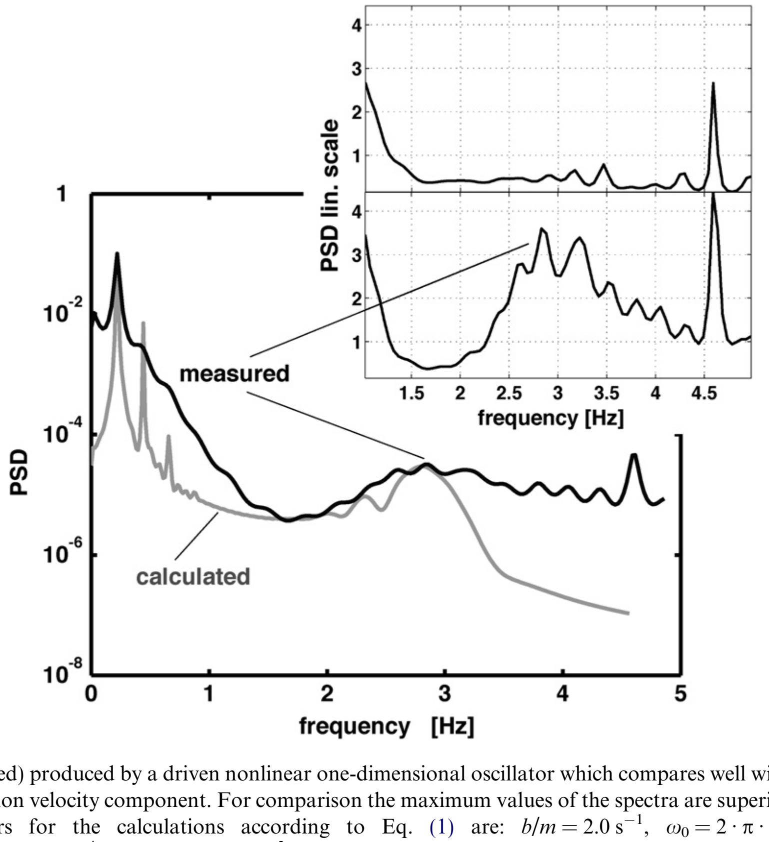


Fig. 1. Spectrum (calculated) produced by a driven nonlinear one-dimensional oscillator which compares well with the measured spectrum of the vertical ground motion velocity component. For comparison the maximum values of the spectra are superimposed and set to a value close to one. Parameters for the calculations according to Eq. (1) are: $b/m = 2.0\ \mathrm{s}^{-1}$, $\omega_0 = 2 \cdot \pi \cdot 2.6$ Hz, $F/m = 0.8\ \mathrm{m\ s}^{-2}$, $\Omega = 2 \cdot \pi \cdot 0.22$ Hz, $A/\omega_0^2 = 1.2 \times 10^4\ \mathrm{s}^{-2}$, $B/\omega_0^2 = 4 \times 10^5\ \mathrm{s}^{-2}\ \mathrm{m}^{-1}$. The insert shows the measured signal after suitable signal to noise ratio improving data processing. The trace on top indicates low and the trace at the bottom high hydrocarbon potential. The measurement locations were about 2 km apart. The peak at about 4.5 Hz is due to a nearby artificial noise source. Note that the frequency separation of the clearly visible fine structure wiggles corresponds to the frequency of the oceanic wave peak which is likely to be caused by nonlinear interactions. Also the higher harmonics of the driving frequency are visible in the measured spectrum.

0.44 Hz. The resonance frequency, which was intentionally set to $\omega_0 = 2\pi \cdot 2.6$ Hz, has been widened by the creation of sum and difference frequencies between $\Omega$ and $\omega_0$ and by the damping term $b/m$.

In order to better understand the meaning of such formal results and their limits, the oscillator parameters and the conditions of the natural environment of a hydrocarbon reservoir have to be related. Two basic poro-mechanical models often used in literature serve as examples [10]. For the linear model (Fig. 2), a bi-conical pore geometry (Fig. 3) is used while a spherical pore shape (Fig. 12) represents the nonlinear case.

## 2. Linear one-dimensional oscillator model

The bi-conical pore geometry has the advantage of providing a linear spring constant for the restoring force which is independent of the dislocation of the pore fill along the $z$-direction. In equilibrium, the capillary forces which are proportional to the length of the oil/rock contact line (ORCL) balance each other.

For small displacements of the liquid, the lengths of both ORCL change in such a way that the related capillary forces $F_z = F_{+z} + F_{-z}$ always add up to a restoring force which enables oscillations.

Neglecting gravity, which would mainly shift the equilibrium position, and assuming nearly filled pores, an oscillation frequency according to the one-dimensional oscillator model can be estimated.

The spring constant

$$f = \frac{dF_z}{dz} = \gamma \frac{2\pi r}{h} \tag{2}$$

and mass

$$m = \frac{2}{3} r^2 \pi h \rho_L \tag{3}$$

lead to the resonance frequency

$$\nu = \frac{1}{2\pi}\sqrt{\frac{f}{m}} = \frac{1}{2\pi h}\sqrt{\frac{6\gamma}{r\rho_L}} \tag{4}$$

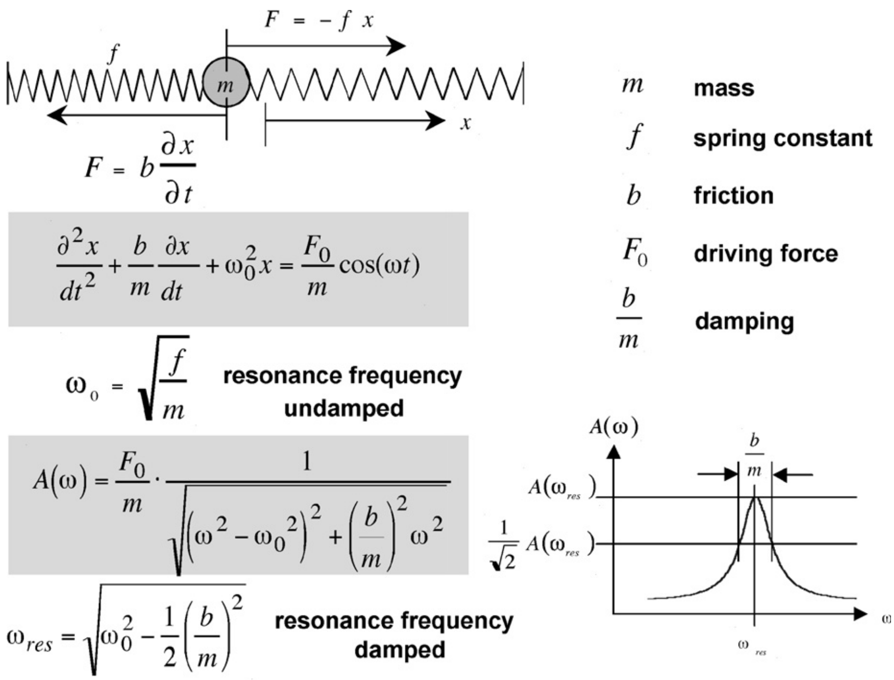


Fig. 2. General description of a driven linear one-dimensional oscillator along the $x$-direction with its second-order differential equation and resonance response function.

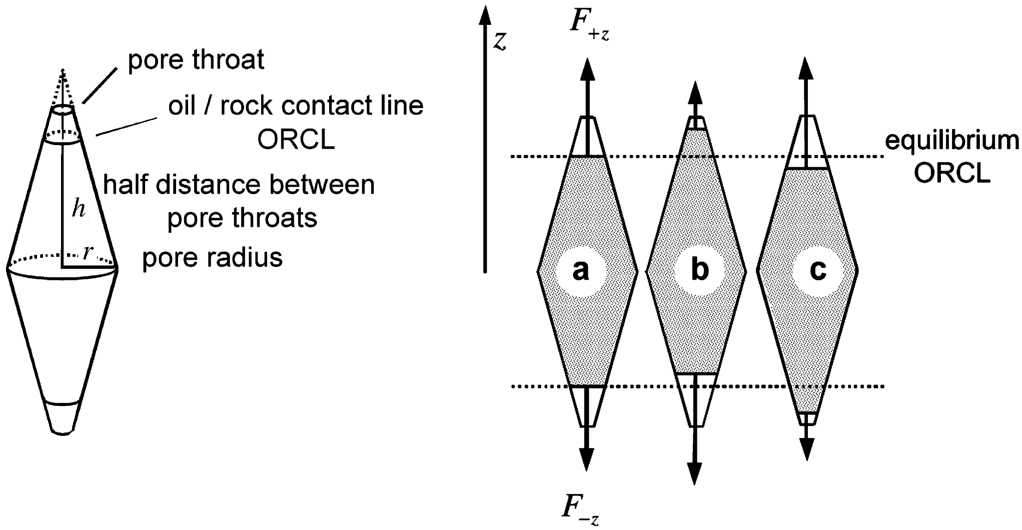


Fig. 3. Schematic representation of a simple bi-conical pore geometry which enables low frequency oscillations of the contained liquid along the $z$-direction. The oil/rock contact line (ORCL) or triple phase line where capillary forces occur is formed between the oil and water phases and the rock material. (a) liquid in equilibrium: the capillary forces $F_{+z}$ in positive and $F_{-z}$ in negative $z$-direction balance each other; (b) Situation after a small displacement of the liquid in the positive $z$-direction: $F_{+z}$ has decreased and $F_{-z}$ has increased compared to the equilibrium. The resulting restoring force drives the liquid back along the negative $z$-direction towards its equilibrium position; (c) same as (b) with dislocation in the negative $z$-direction.

The observed value of $v = 3$ Hz is compatible with realistic values of the relevant parameters given in Table 1. Fig. 4 shows, as an example, how the sharp-peaked spectrum of a single oscillator approaches the wider observed shape as a function of the width "sigma" of the assumed log-normal parameter distribution.

## 3. Navier–Stokes equations

In order to verify the approximations used in the one-dimensional oscillator model, the Navier–Stokes equations which are mainly based on fundamental ab initio concepts such as conservation laws, constitutive equations and boundary conditions for the liquid filled bi-conical pore are numerically solved.

### 3.1. Code

TransAT [11] is a finite-volume multi-physic code solving the multi-fluid Navier–Stokes equations. The code uses multi-block, structured meshes along with a message-passing parallel algorithm. The grid arrangement is collocated and can handle general curvilinear grids. Multiphase flows are computed using the particle tracking approach, or interface tracking techniques. The flow is modeled as one fluid having variable material properties according to a phase indicator function which distinguishes the gas phase regions from the liquid

Table 1
Common parameter values

| | |
|---|---|
| Pore radius, $r$ | $1 \times 10^{-3}$ m |
| Half distance between pore throats, $h$ | $5 \times 10^{-3}$ m |
| Surface tension of oil, $\gamma$ | $10^{-3}$ N m$^{-1}$ |
| Density of oil, $\rho_L$ | $8 \times 10^{2}$ kg m$^{-3}$ |
| Viscosity, $\mu$ | $6 \times 10^{-4}$ kg s$^{-1}$ m$^{-1}$ |
| Low viscosity, $\mu$ | $6 \times 10^{-5}$ kg s$^{-1}$ m$^{-1}$ |
| Resonance frequency, $\omega_0$ | $3 \cdot (2 \cdot \pi)$ Hz |

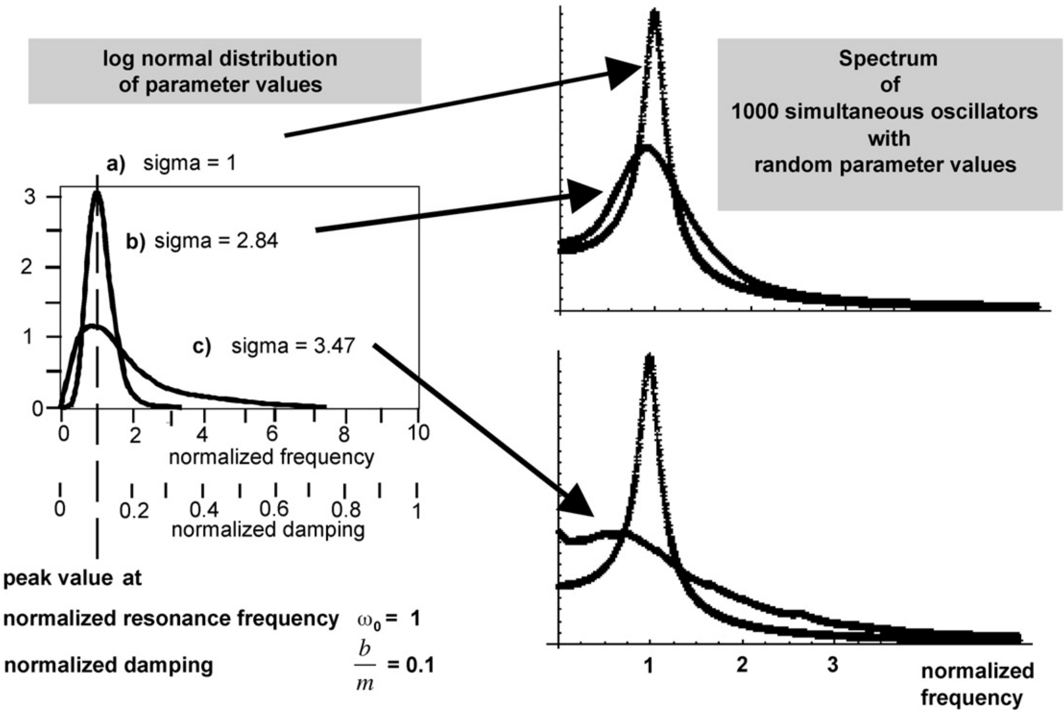


Fig. 4. Numerical simulation of the superimposed spectrum of 1000 linear harmonic oscillators for three different parameter distributions: (a) all oscillators with normalized resonance frequency at $\omega_0 = 1$ and damping term $b/m = 0.1$; (b) both resonance frequency and damping vary according to a log-normal distribution with sigma = 2.84; (c) both resonance frequency and damping vary according to a broad log-normal distribution with sigma = 3.47.

phase. Both the level-set and the volume-of-fluid interface tracking methods (ITM) can be employed in the code to track evolving interfaces.

### 3.2. Transport equations

The incompressible heat and fluid flow equations expressed within the single-fluid formalism take the following form

$$\nabla \cdot u = 0 \tag{5}$$

$$\frac{\partial}{\partial t}(\rho \cdot u) + \nabla \cdot (\rho \cdot u \cdot u - \sigma) = F_s + F_b + F_{tl} \tag{6}$$

where $\rho$ is the density of the liquid pore fill, $u$ is the velocity vector of the pore fill and the RHS terms in the momentum equation (Eq. (6)) represent the surface tension expressed by Eq. (8) below, body forces and the triple-line wall contribution respectively and $\sigma = \tau - p \cdot I$ is the Newtonian viscous stress tensor with its share component $\tau_w$ parallel to the wall and its pressure induced component $p \cdot I$ ($p$: pressure, $I$: identity matrix). Isothermal conditions are assumed.

### 3.3. The level-set method

In our simulations, the oscillation of oil in one pore is simulated using a two-phase flow description of the oil–water system inside the pore. The description uses the level-set (LS) method to define the interface between the two fluids and to combine the dynamics of the two phases to get a consolidated Navier–Stokes equation. Because the simulation captures the dynamics of forced oscillation in one pore – in principle – we are not simulating porous media.

In the LS method, the interface between immiscible fluids is represented by a continuous function $\varphi$, representing the distance to the interface which is positive on one side and negative on the other. The two fluids can now be identified by the location of the interface representing the zero level. The LS evolution equation is

$$\frac{\partial \varphi}{\partial t} + u \cdot \nabla \varphi = 0 \tag{7}$$

Material properties such as the density, the viscosity, and the thermal conductivity are updated locally based on $\varphi$ and smoothed across the interface using a smooth Heaviside function. The fact that $\varphi$ is a continuous function across the interface helps to determine the normal vector $\boldsymbol{n}$ to the interface, and thereby the surface curvature $\kappa$ required for the determination of the surface tension,

$$F_{\mathrm{s}} = \gamma \kappa \delta_{\mathrm{s}} \boldsymbol{n} \tag{8}$$

where $\gamma$ is the surface tension of the fluid and $\delta_{\mathrm{s}}$ is the Dirac delta function located at the interface.

### 3.4. Simulation setup and results

The bi-conical pore is setup as an axisymmetric body of revolution as shown in Fig. 5. The pore is initialised with oil in the center and water at the edges. A sinusoidal forcing is applied to the flow domain of given amplitude (0.05 mm) and frequency. The simulation is run for a fixed number of cycles and the motion of the center-of-mass of the oil is calculated. By comparing the amplitude and phase of the oscillation with the imposed oscillation, the amplitude and phase response of the system is computed. The Navier–Stokes equations and the level-set advection equation are numerically solved using the third-order Runge–Kutta explicit scheme for time integration. The convective fluxes are discretised using the higher-order bounded HLPA scheme. The diffusive fluxes are discretised using the second-order central scheme.

Two pores with center diameter of 3 mm and 1 mm were simulated for a range of frequencies (0.5–10 Hz). Further refinement in the frequencies was performed near the observed resonance frequency for the 3 mm diameter case. Fig. 6 shows the amplitude and phase response for the 3 mm diameter pore. Resonance is observed at approximately 1 Hz for a viscosity of $\mu = 6 \times 10^{-4}\,\mathrm{kg\,s^{-1}\,m^{-1}}$. For a lower viscosity ($\mu = 6 \times 10^{-5}\,\mathrm{kg\,s^{-1}\,m^{-1}}$) the resonance frequency is shifted to approximately 1.7 Hz. As expected the phase angle undergoes a 90° shift at resonance. For the 1 mm pore, resonance is observed at approximately 4.6 Hz (Fig. 7).

### 3.5. Forces acting on the oil drop

The different forces acting on the oil drop at two different frequencies (1 Hz and 3 Hz) for the 3 mm pores are shown in Figs. 8a and b. The forces acting on the oil drop are schematically shown in Figs. 5, namely the wall pressure and viscous shear, the inertial force, the triple line force at the ORCL, the surface tension force, and the imposed sinusoidal oscillation. Different forces have different amplitude and phase relationships to the

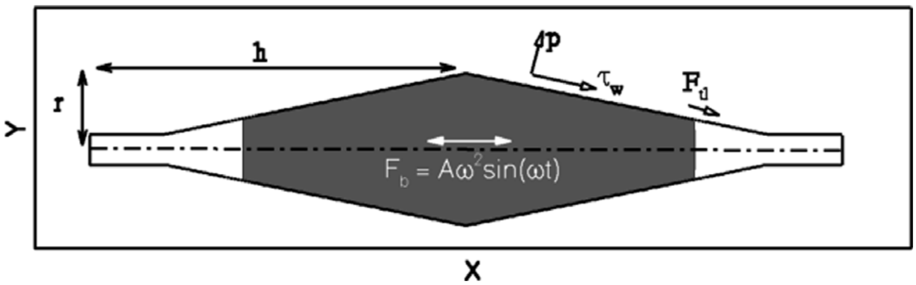


Fig. 5. Bi-conical pore geometry with forces acting on the oil drop. For the calculations two pore shapes with of $r = 1$ mm, $h = 1.5$ mm and $r = 3$ mm, $h = 4.5$ mm were used. The external force was adjusted for a non-resonant displacement of $A = 2 \times 10^{-6}$ m for the 1 mm pore diameter and of $A = 2 \times 10^{-5}$ m for the 3 mm pore diameter.

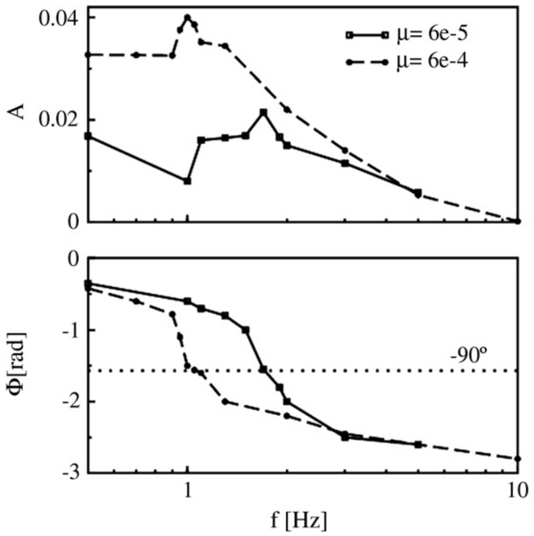


Fig. 6. Amplitude $A$ (mm) and phase response $\Phi$ (rad) for 3 mm pore diameter. Viscosity $\mu = 6 \times 10^{-4}\,\mathrm{kg\,s^{-1}\,m^{-1}}$ and $\mu = 6 \times 10^{-5}\,\mathrm{kg\,s^{-1}\,m^{-1}}$.

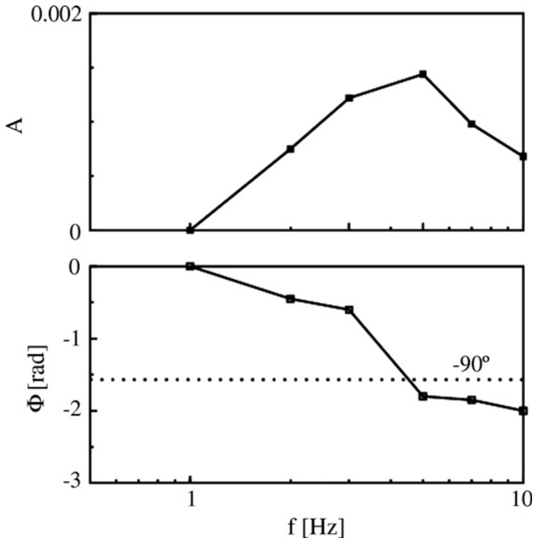


Fig. 7. Amplitude $A$ (mm) and phase response $\Phi$ (rad) 1 mm pore diameter. $\mu = 6 \times 10^{-4}\,\mathrm{kg\,s^{-1}\,m^{-1}}$.

imposed oscillation. The wall pressure is typically in phase with the imposed oscillation, whereas the viscous shear lags the imposed oscillation.

The variation of the magnitudes of the different forces with respect to the imposed frequency normalized by the imposed oscillation magnitude is shown in Fig. 9. It can be observed that the forces generally reduce with increasing frequency. They also show a small increase/decrease in amplitude near the resonance frequency (approximately 1 Hz).

## 4. Comparison of calculated pore oscillation behaviour to a linear harmonic oscillator

Fig. 10 shows the frequency dependence of amplitudes and phases calculated by the numerical Navier–Stokes model (NSM) and the linear harmonic oscillator model (LHOM) for three cases: pore of 1 mm radius

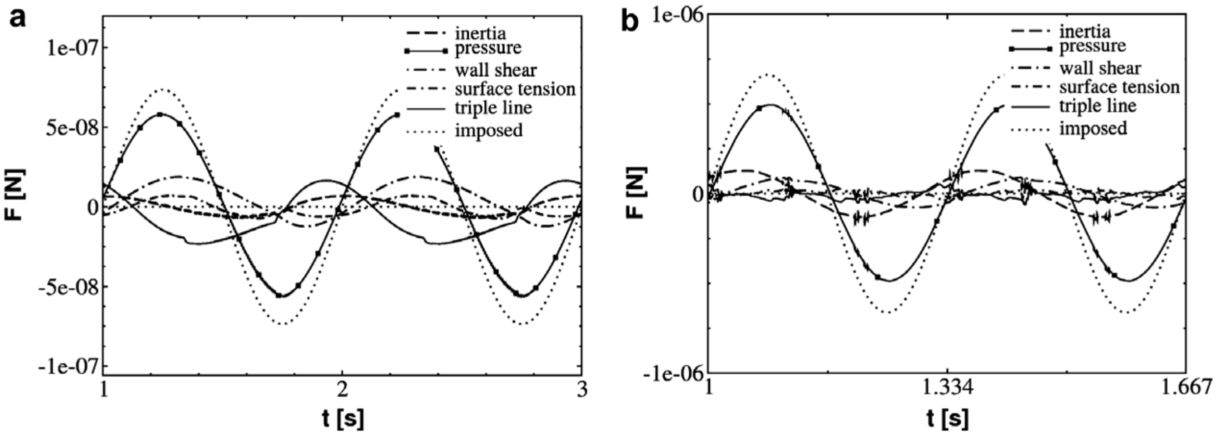


Fig. 8. (a) Forces acting at 1 Hz on oil drop and (b) forces acting at 3 Hz on oil drop. The little bursts are numerical oscillations due to the contact line moving from one finite volume to another. Special treatment is done only on one control volume for the dynamic contact line model.

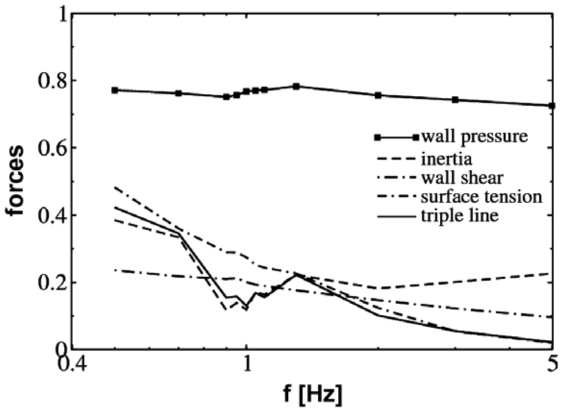


Fig. 9. Variation of forces with respect to frequency. The forces add up to one considering that the triple line force is a negative contribution and the surface tension force is an internal force of which the resulting net force is represented by the triple line force.

and 3 mm radius with two different viscosities. For each case two fits are indicated, one for good agreement in the maximum amplitude region and one for good agreement at frequencies far below and above resonance. The oscillator parameters for each case and fit are listed in Table 2.

The expressions for the response of a linear harmonic oscillator are

$$A(\omega) = \frac{F_0}{m} \frac{1}{\sqrt{(\omega_0^2 - \omega^2) + \left(\frac{b}{m}\right)^2 \omega^2}} \tag{9}$$

for the amplitude and

$$\Phi = -\arctan\left(\frac{\frac{b}{m}\omega}{\omega_0^2 - \omega^2}\right) \tag{10}$$

for the phase with excitation acceleration $\frac{F_0}{m}$, resonance frequency $\omega_0$ and damping $\frac{b}{m}$.

For a cylindrically shaped pore the frictional term can be deduced from the Hagen–Poiseuille law of flow resistance through a capillary. There the frictional force $F_R$ is proportional to the volume flow $\frac{dV}{dt}$ according to

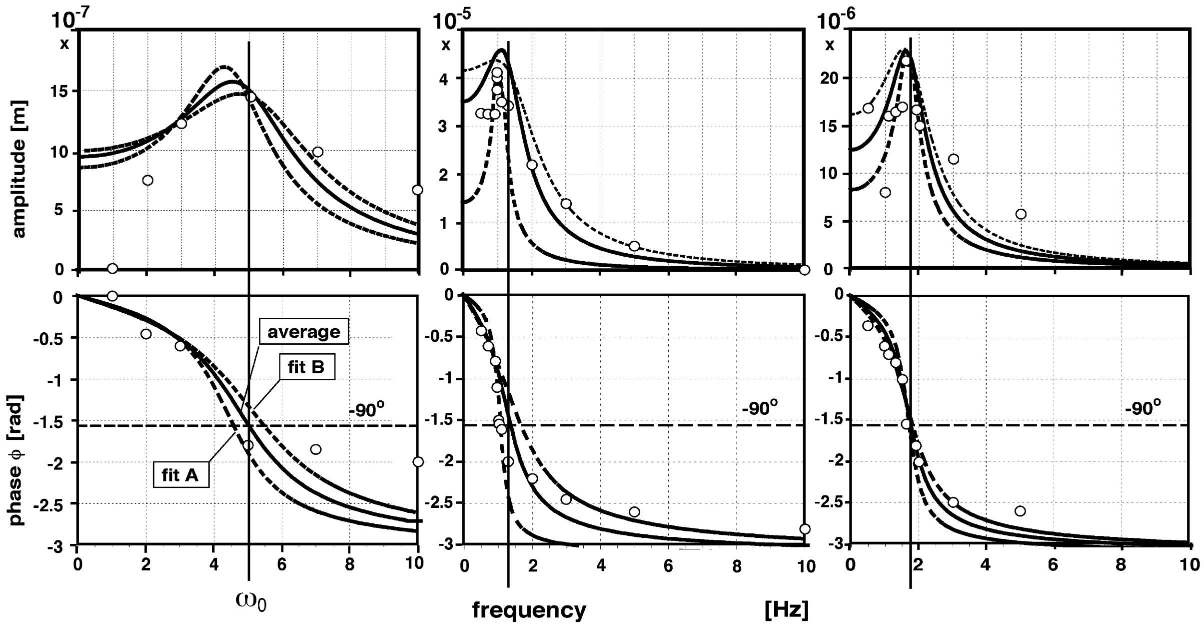


Fig. 10. Amplitudes and phases calculated by the Navier–Stokes model (NSM) and the linear harmonic oscillator model (LHOM) for a pore of 1 mm radius (left) and 3 mm radius (middle: same viscosity as 1 mm pore; right: lower viscosity). Open circles: calculated by NSM; fit A dashed line: LHOM fitted for good agreement around the resonance frequency; fit *B* dashed line: LHOM fitted for good agreement at the wings; solid line: average of fit *A* and fit *B*.

Table 2
Harmonic oscillator parameters which approximate the pore oscillation behaviour

| | 1 mm pore radius | | | 3 mm pore radius | | | 3 mm pore radius low viscosity | | |
|---|---|---|---|---|---|---|---|---|---|
| | Fit *B* | Fit *A* | Average | Fit *B* | Fit *A* | Average | Fit *B* | Fit *A* | Average |
| Excitation ($10^{-2}$ m s$^{-2}$) | 3 | 1.8 | 2.4 | 12 | 1.7 | 6.85 | 5.5 | 2.5 | 4.0 |
| Resonance frequency (Hz) | 5.5 | 4.6 | 5.05 | 1.7 | 1.1 | 1.4 | 1.85 | 1.75 | 1.8 |
| Damping (s$^{-1}$) | 2.0 | 1.2 | 1.6 | 1.0 | 0.18 | 0.59 | 0.7 | 0.32 | 0.51 |

$$F_{\mathrm{R}} = A \cdot \Delta p = A \cdot \frac{\mathrm{d}V}{\mathrm{d}t} \cdot R \tag{11}$$

with the capillary cross section $A$ and the flow resistivity

$$R = \frac{8\mu l}{\pi r^4} \tag{12}$$

On the other hand, for the oscillator the frictional force is

$$F_{\mathrm{R}} = b\frac{\mathrm{d}z}{\mathrm{d}t} \tag{13}$$

Combining Eqs. (11)–(13) leads to

$$b\frac{\mathrm{d}z}{\mathrm{d}t} = A \cdot \frac{\mathrm{d}V}{\mathrm{d}t} \cdot \frac{8\mu l}{\pi r^4} = A \cdot A \cdot \frac{\mathrm{d}z}{\mathrm{d}t} \cdot \frac{8\mu l}{\pi r^4} = A \cdot \frac{\mathrm{d}z}{\mathrm{d}t} \cdot \frac{8\mu l}{r^2} \tag{14}$$

and therefore

$$\frac{b}{m} = \frac{1}{\rho_{\mathrm{L}} A l} A \cdot \frac{\mathrm{d}z}{\mathrm{d}t} \cdot \frac{8\mu l}{r^2} = \frac{8\mu}{r^2 \rho_{\mathrm{L}}} \tag{15}$$

In case of a tapered tube, this value has to be corrected for the energy required by the radial displacement of the liquid flowing through the capillary. However, due to the symmetric tapered shape of the bi-conical pore this correction cancels out for a full oscillation cycle of the fluid along the $z$-direction, but the average radius has to be adjusted to about $r/2$ for a nearly saturated pore. The dependence of the frictional term of the linear harmonic oscillator in the case of a saturated bi-conical pore can therefore be written as

$$\frac{b}{m} = \frac{32\mu}{r^2\rho_\mathrm{L}} \tag{16}$$

The comparison of the resonance frequency and the frictional term between the "straight forward" linear oscillator (LO), where parameter values from Table 1 have been used, and the average fit of a linear oscillator to the Navier stokes calculations (LONS) using the same parameter values is shown in Table 3.

The resonance frequencies of the LONS are consistently about a factor of 2 larger than for the LO. However, they compare well within the same order of magnitude also for different pore sizes. Therefore Eq. (4) appears to be a good approximation which could even be improved by an "empirical factor" of 2.

Regarding the frictional term, the approximation (Eq. (16)) gives the right order of magnitude, but for the LONS the dependence on viscosity is much less than for the LO.

## 5. Observation of the signals at the surface

In order to explore the feasibility of the explanation by pore level oscillations, the following approximation is made.

Assuming frequency dependent forces in the order of a fraction $c$ of the capillary forces for each pore, the measured velocity at the earth surface due to the coherent oscillations of the pores in the hydrocarbon containing porous layer of thickness $d$ at depth $D$ as indicated in Fig. 11 can be estimated.

The total force $F_\mathrm{T}$ represents the coherent sum of the fractional forces of the $n$ pore oscillators

$$F_T = nF_z, \quad n = \frac{3\eta dA}{2r^2\pi h}, \quad F_z = c \cdot \gamma \cdot 2\pi r \sin(\omega t) \tag{17}$$

This force accelerates the mass $M = D\,A\rho_\mathrm{R}$ of the overlaying rock material according to Newton's law

$$F_T = M\frac{\mathrm{d}^2 z}{\mathrm{d}t^2} \tag{18}$$

which leads to a measurable velocity at the earth surface on top of the reservoir of

$$\frac{\mathrm{d}z}{\mathrm{d}t} = -\frac{n}{M\omega} c \cdot \gamma \cdot 2\pi r \cos(\omega t) = -v_z \cos(\omega t) \tag{19}$$

Table 3
Comparison of resonance frequency and frictional terms between the linear oscillator (LO) and the average fit of a linear oscillator to the Navier–Stokes calculations (LONS)

| | LO | LONS |
|---|---|---|
| 1 mm | | |
| Resonance frequency (Hz) | 2.76 | 5.5 |
| Frictional term $b/m$ (N s m$^{-1}$ kg$^{-1}$) | 24 | 3.2 |
| 3 mm | | |
| Resonance frequency (Hz) | 0.53 | 1.4 |
| Frictional term $b/m$ (N s m$^{-1}$ kg$^{-1}$) | 2.7 | 1.2 |
| 3 mm, low viscosity | | |
| Resonance frequency (Hz) | 0.53 | 1.8 |
| Frictional term $b/m$ (N s m$^{-1}$ kg$^{-1}$) | 0.27 | 1.0 |

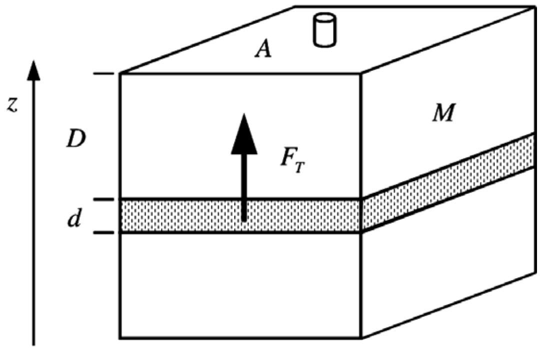


Fig. 11. Simple model for the occurrence of low frequency seismic signals due to pore liquid oscillations. At the surface a seismic sensor measures the surface motion.

The value

$$v_z = \frac{n}{M\omega} c \cdot \gamma \cdot 2\pi r = \frac{3\eta d c \gamma}{r h \omega D \rho_R} \tag{20}$$

is compatible with typical measured values of the vertical component of the ground velocity of about $10^{-6}$ m $s^{-1}$ for the realistic parameter values listed in Table 4.

The parameter $c$ represents the fraction of the capillary force which is assumed to contribute to the total force which produces measurable signals at the surface. The value of $c$ has to be compared to the frequency dependent forces calculated by the Navier–Stokes equations (Fig. 9): the ‘‘triple line force’’ and the ‘‘inertia’’, which are the same forces phase shifted by half an oscillation period (Fig. 8). The difference of these forces between ‘‘on’’ and ‘‘off’’ resonance is about 10% of the total force. The value of $c = 10^{-2}$ therefore represents a rather conservative estimation which could be chosen closer to $c = 10^{-1}$.

## 6. Nonlinear oscillation due to a spherical pore shape

As the initial example has shown the explanation of the fine structure wiggles shown in Fig. 1 may be explained by the occurrence of nonlinearity in the above model by allowing for a more general pore shape, e.g. spherical as shown in Fig. 12. This defines a more general, nonlinear spring constant in a natural way. Such nonlinearities actually provide the more common case in nature ([10] and references to Oh and Shatterly (1979) and Payatakes et al. (1980) therein).

The nonlinear spring constant depending on the filling level $z_0$ is given by

$$f = \frac{\mathrm{d}}{\mathrm{d}z}(\gamma 2\pi r(z)) = 2\pi\gamma \frac{\mathrm{d}}{\mathrm{d}z}\sqrt{r^2 - (z_0 + z)^2} = -\frac{2\pi\gamma(z_0 + z)}{\sqrt{r^2 - (z_0 + z)^2}} \tag{21}$$

which leads to the nonlinear one-dimensional differential equation

$$\frac{\mathrm{d}^2 z}{\mathrm{d}t^2} + \frac{b}{m}\frac{\mathrm{d}z}{\mathrm{d}t} + \frac{2\pi\gamma(z_0 + z)z}{m\sqrt{r^2 - (z_0 + z)^2}} = \frac{F_0}{m}\cos(\omega t) \tag{22}$$

Table 4
Common parameter values for reservoir structure

| | |
|---|---|
| Depth of hydrocarbon containing formation, $D$ | $10^3$ m |
| Hydrocarbon layer thickness, $d$ | 20 m |
| Density of rock material, $\rho_R$ | $2 \times 10^3$ kg m$^{-3}$ |
| Porosity, $\eta$ | 0.2 |
| Fraction of maximum capillary force at ORCL $= 2 \cdot \pi \cdot r$, $c$ | $10^{-2}$ |

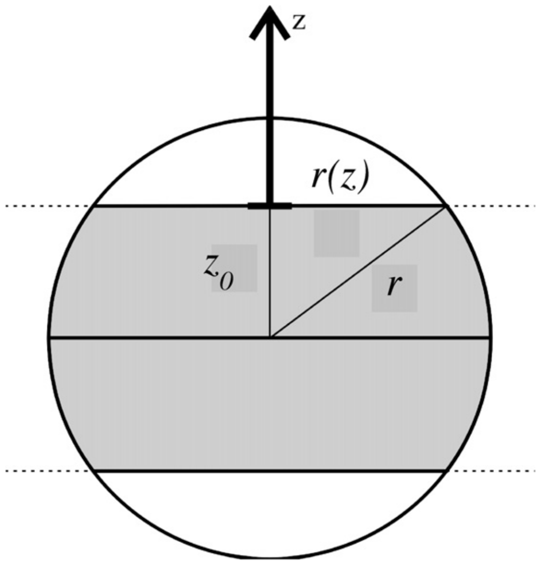


Fig. 12. Schematic representation of a spherical pore geometry which enables low frequency oscillations of the contained liquid along the $z$-direction. Similar to the bi-conical case shown in Fig. 3, the liquid surface boundary forms the oil/rock contact line and the restoring capillary forces drive the liquid back along the $z$-direction towards its equilibrium position after an initial dislocation. While the bi-conical pore geometry leads to a linear spring constant for the restoring motion, the spherical pore geometry results in a nonlinear spring constant that depends on the dislocation and therefore leads to a nonlinear restoring motion.

The filling-level dependent oscillation mass and frequency are

$$m = \frac{4}{3}\pi r^3 \rho_{\mathrm{L}} \frac{(3r^2 z_0 - z_0^3)}{2r^3} \tag{23}$$

and

$$\omega_0 = \sqrt{f/m} \approx \sqrt{\frac{2\pi\gamma z_0}{m\sqrt{r^2 - z_0^2}}} \tag{24}$$

The synthetic spectra obtained from the nonlinear model are displayed in Fig. 13 for different filling levels. The single peak spectrum of the linear case splits up into several peaks which are separated by the driving oscillation frequency.

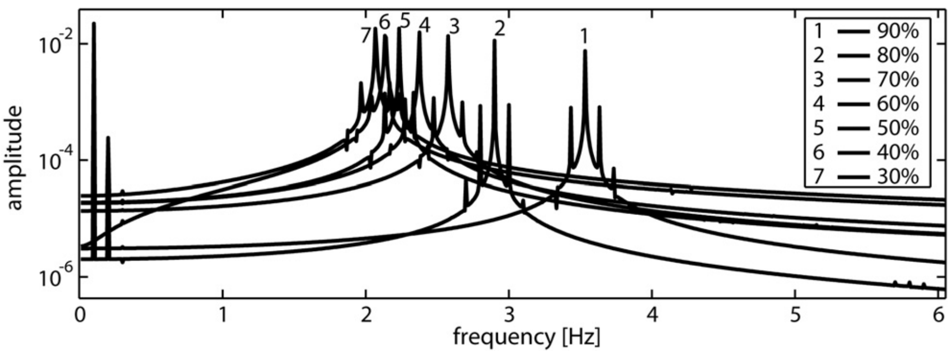


Fig. 13. Spectrum of nonlinear oscillations in a spherical pore for different oil saturations. Pore liquid filling levels $z_0$ are between 0.3 and 0.9. The frequency spacing of the multiple peaks is a typical feature of nonlinear systems and corresponds to the frequency of the driving oscillation at 0.1 Hz, which also produces its own overtone at 0.2 Hz. For demonstration reasons, the damping was set to zero which leads to sharper peaks.

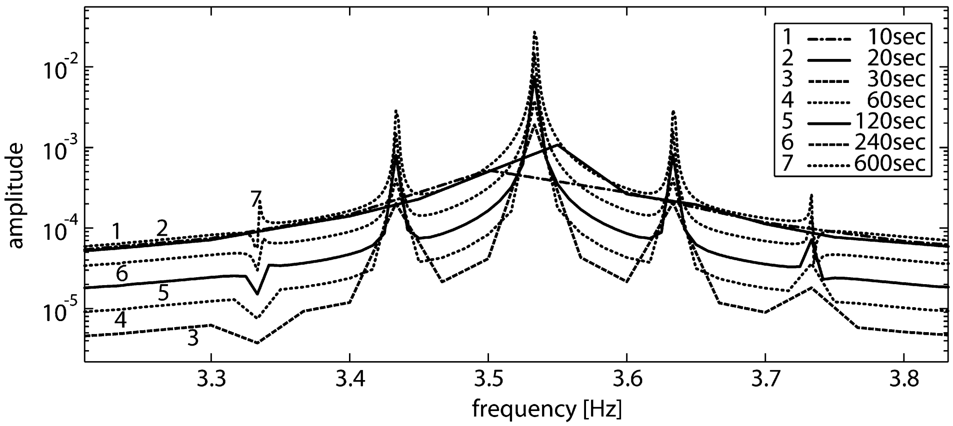


Fig. 14. Development of the spectrum of nonlinear oscillations in a spherical pore during 600 s for filling level $z_0 = 0.9$ of the pore liquid. The frequency spacing of the multiple peaks is a typical feature of nonlinear systems and corresponds to the frequency of the driving oscillation at 0.1 Hz. Natural oscillation frequency of pore: $v = 3.527$ Hz, mass of liquid in pore $m = 2.64 \times 10^{-5}$ kg.

The frequency of the spectrum shifts toward larger values as the oil saturation increases. Note that these features need a certain transient time to build up, as is demonstrated in Fig. 14.

## 7. Discussion

The observed oscillations seem to commonly appear in the low frequency range between 1 and 10 Hz at all investigated sites independent of the hydrocarbon reservoir thickness. This favours the microscopic oscillator model compared to a reservoir thickness dependent macroscopic resonator model. In order to obtain sufficiently low resonance frequencies the "spring constant" has to be small which requires a low value of the surface tension $\gamma$, a large oscillating mass and a large value of the aspect ratio $h/r$. Surface tension and interfacial tension values in pore media are not well investigated [10] but can be orders of magnitude lower than the literature values of water ($73 \times 10^{-3}$ N/m) or crude oil ($20 \times 10^{-3}$ N/m) due to contamination, increased temperatures and contact of the oil to water as an additional liquid medium in the pores. Water wetted pore surfaces also lower interfacial tension and avoid pinning effects of the ORCL [10]. A large oscillating mass requires large pore diameters or the coupling of several smaller pores.

The assumption of coherent superposition of frictional forces requires either spatially coherent excitation (e.g. by the strong long-wavelength oceanic wave component of the geological background noise spectrum) or a coherent coupling mechanism between the pores either through the liquid or the solid phases. In the case of low frequency oceanic wave excitation this assumption is well satisfied. The coupling of the pore level oscillations to the rock material and the propagation of the seismic wave to the surface is presently under investigation. Also other effects that may create similar signals, e.g. such as trapping of surface waves in near surface geological structures [12] are the subject of extensive numerical modeling.

## 8. Conclusions

It has been shown that the phenomenological model of a driven one-dimensional linear and nonlinear oscillator can provide a natural interpretation of characteristic spectral features empirically attributable to hydrocarbon reservoirs. The basic requirement for oscillations, the presence of a restoring force on the pore scale, has been derived from first principles using Navier–Stokes Equations. Good agreement between the numerical results and the observations is achieved for realistic parameter values using the dominant part of the ever present background wave spectrum, the seismic wave field around 0.1–0.2 Hz caused by oceanic waves, as the driving force for the oscillations.

## Acknowledgements

We thank Stefan Schmalholz, Department of Earth Sciences, ETH Zurich, Switzerland and Yuri Podladchikov, Physics of Geological Processes, University of Oslo, Norway, for their fruitful discussions and suggestions.

## References

[1] Holzner R, Eschle P, Zürcher H, Lambert M, Graf R, Dangel S, et al. Applying microtremor analysis to identify hydrocarbon reservoirs. First Break 2005;23:41–9.
[2] HyMAS is a trade mark of Spectraseis Technologie AG, Switzerland.
[3] Dangel S et al. Phenomenology of tremor-like signals observed over hydrocarbon reservoirs. J Volcanol Geotherm Res 2003;128:135–58.
[4] Goloshubin GM et al. Slow wave phenomenon at seismic frequencies. In: 63th annual international SEG meeting, Washington (DC), SL4.6; 1993. p. 809–11.
[5] Al Dulaijan A, Van Mastrigt P, Al-Somali F, Saadaoui K, Morris I. New technology applications in the Rub Al-Khali Desert. In: Proceedings of GEO 2006 middle east conference and exhibition, Bahrain, March 27–29, 2006.
[6] Rached G. Surface passive seismic measurements in Kuwait (Presentation A27).Suntsov AE, Aroutunov SL, Mekhnin AM, Meltchouk BY. Passive infra-frequency microseismic technology – experience and problems of practical use (Presentation A25).Akrawi K, Bloch G. Application of passive seismic (IPDS) surveys in Arabian Peninsula (Presentation A28).Kouznetsov OL, Chirkine IA, Volkov AV, Meltchouk BY, Vorobiev AS, Joukov AS, et al. Applying seismic location of emission centers (Slec) to monitor the production in oil-and-gas fields. In: Proceedings of EAGE workshop ‘‘passive seismic: exploration and monitoring applications’’, Dubai, United Arab Emirates, 10–13 December 2006 (Presentation A36).
[7] Kuznetsov OL, Grafov BM, Aroutunov SL, Suntsov AE. About the theory of ANCHAR method. Seismic Exploration Technologies II Geofizika special issue, 2003, p. 103–7. [in Russian].
[8] Macedo I, Dittz R, Santos de Oliveira A, Holzner R, Graf R. Observation and modeling of seismic background noise. In: Ninth international congress of the Brazilian Geophysical Society, 11–14 September 2005, Salvador, Bahia, Brazil.
[9] Holzner R, Eschle P, Meier PF, Dangel S. Linear model for low frequency pore liquid oscillations observed in hydrocarbon microtremor analysis (HyMAS). GEO 2006, 27–29 March 2006, Bahrain.Holzner R, Eschle P, Frehner M, Schmalholz S, Podladchikov Y. Hydrocarbon microtremors interpreted as nonlinear oscillations driven by oceanic background waves. In: EAGE 68th conference & exhibition, Vienna, Austria, 12–15 June 2006.
[10] Hilpert M et al. Capillarity-induced resonance of oil blobs in capillary tubes and porous media. Geophysics 2000;65:874–83.
[11] TransAT is a protected trademark. <www.ascomp.ch/transat.html>.
[12] Lomnitz Cinna, Meas Yunny. Huygens’ principle: the capture of seismic energy by a soft soil layer. Geophys Res Lett 2004;31:L13613.